Journal of Science and Technology – Engineering and Technology for Sustainable Development
Volume 36, Issue 5, November 2026, 094–102

Design and Development of a Constant Volume Combustion Chamber for Fuel Spray and Combustion Studies under Compression Ignition Engine Conditions

Thu Hoang Van[1,2], Tuyen Pham Huu[1,*], Nghia Do Van[1] , Tuan Nguyen Huu[3]
[1]*School of Mechanical Engineering, Hanoi University of Science and Technology, Ha Noi, Vietnam*
[2]*Vinh University of Technology Education, Nghe An, Vietnam*
[3]*Faculty of Mechanical Engineering, Thuyloi University, Ha Noi, Vietnam*
[*]*Corresponding author email: tuyen.phamhuu@hust.edu.vn*

Abstract

Constant Volume Combustion Chambers (CVCCs) are widely used to investigate fuel spray and combustion processes under well-controlled thermodynamic conditions, providing an effective platform for fundamental combustion research. However, the design and experimental validation of a compact, robust, and cost-effective CVCC capable of reproducing relevant compression ignition (CI) engine conditions remain important for laboratory-scale combustion investigations. The paper presents the design, fabrication, and experimental validation of a CVCC developed for investigating diesel fuel spray and combustion under elevated pressure and temperature conditions representative of CI engine operation. The design considered chamber geometry, dimensions, materials, durability, efficiency, and operational safety. Structural and thermal analyses were performed using finite element methods in ANSYS to ensure mechanical strength and thermal stability while maintaining a compact and cost-effective configuration. The simulations predicted maximum Von Mises stresses of 20.4 MPa in the chamber body and 27.7 MPa in the flange cover, with a maximum deformation of only 0.002 mm, confirming adequate structural integrity under the design operating conditions. The CVCC was fabricated using locally available manufacturing processes and integrated with gas supply, electrical heating, pressure measurement, optical diagnostics, and a common-rail diesel injection system. Experimental results demonstrated stable fuel spray development and combustion under elevated pressure and temperature conditions. Measurements of flame evolution, in-chamber pressure, and heat release rate confirmed reliable operation and suitability for combustion diagnostics. The developed CVCC provides a controlled experimental platform for fundamental investigations of CI combustion and offers a flexible basis for studying fuel spray, ignition, combustion characteristics and the effects of alternative and low-carbon fuels.

Keywords: Constant volume combustion chamber, spray visualization, diesel combustion, compression ignition engine.

1. Introduction

Over the last decade, the use of optical methods to visualize phenomena in internal combustion engines such as fuel injection, mixing, combustion, and emission formation, has developed rapidly. Optical accessible engines and constant volume combustion chambers (CVCC) have been widely used to investigate these phenomena. CVCCs are mainly used to simulate injection and combustion events when the piston is near top dead center (TDC) and to analyze the combustion characteristics of different fuels under premixed, partially premixed or direct injection conditions. The use of CVCCs offers the advantage of easily varying combustion parameters such as the air-fuel ratio, residual gas fraction, initial chamber pressure and temperature, injector, and spark plug positions, electrode gap and spark characteristics. Regarding CVCC configurations, various designs have been developed. The most common chamber geometries are cubic, cylindrical, and spherical. Cylindrical chambers can be designed in two configurations. In the first configuration, the injection axis is perpendicular to the cylinder axis, which is referred to as a horizontal CVCC in this work. In the second configuration, the injection axis is aligned with the cylinder axis, which is referred to as a vertical CVCC. The advantages of the first configuration include easier placement, clamping and sealing of the optical window, whereas the main advantage of the second configuration is its greater similarity to the geometry of an actual engine cylinder. However, when the vertical configuration is used, the optically accessible window is generally smaller than that of the horizontal configuration, making glass window mounting more difficult and potentially altering the original cylindrical geometry of the combustion chamber [1].

Worldwide, several studies have investigated and experimentally tested constant volume combustion chambers. Among studies employing finite element analysis for CVCC design, Alireza Hajialimohammadi *et al.* [1] designed and verified the structural integrity of the combustion chamber and quartz windows under

p-ISSN 3093-3242
e-ISSN 3093-3579
https://doi.org/10.51316/jst.195.etsd.2026.36.5.12
Received: Jun 12, 2026; Revised: Aug 14, 2026;
Accepted: Aug 27, 2026; Online: Oct 28, 2026

high pressure loading and combustion induced thermal shock, with a maximum design pressure of 100 bar. Ronnachart Munsin *et al.* [2] also verified the structural integrity of the combustion chamber and quartz windows at a design pressure of 100 bar. In their study, a pre-combustion technique was employed to generate high temperature and high pressure conditions representative of those in compression ignition engines. Muteeb Ul Haq, Jafry *et al.* [3] developed a constant volume spray chamber (CVSC) to experimentally investigate the effects of ambient and injection pressures on macroscopic spray characteristics. Vo Tan Chau *et al.* [4] designed a CVCC and evaluated its structural strength and deformation using ANSYS at a pressure of 200 bar. However, the CVCC system was neither fabricated nor experimentally validated. Nguyen Phi Truong *et al.* [5] developed a CVCC model to investigate the effects of various parameters on the combustion characteristics of a homogeneous charge compression ignition (HCCI) engine.

Based on the above review, most CVCC systems have been designed for specific research objectives, such as spray visualization, combustion studies, or structural optimization. In the present study, a horizontal cylindrical CVCC was developed as an integrated experimental platform incorporating structural design, finite element analysis and experimental verification, and optical visualization of spray development and combustion processes. The developed CVCC is capable of establishing an initial chamber pressure of up to 60 bar and an initial chamber temperature of up to 800 K through compressed gas charging and electrical resistance heating, without requiring a pre-combustion process or pilot-fuel combustion. The gas charging and heating systems were designed independently, allowing the initial pressure and temperature conditions to be controlled according to the experimental requirements. Combined with optical access and a data acquisition system, the developed platform enables the investigation of spray and combustion characteristics of different fuels under conditions representative of compression-ignition (CI) engines. The structural integrity of the combustion chamber was evaluated using ANSYS, and the safe operation of the developed CVCC was subsequently verified through experimental testing under the specified temperature and pressure conditions.

2. Numerical Calculation and Design of a Constant Volume Combustion Chamber

2.1. Constant Volume Chamber and the Arrangement of the Optical Equipment

Fig. 1 presents a schematic diagram of the CVCC system developed in this study, comprising a combustion chamber, a fuel system, a compressed-gas supply system, a temperature control system, a pressure data acquisition system, and a data display and processing system. The combustion chamber was fabricated from stainless steel with a cylindrical configuration to ensure safe operation under high-temperature and high-pressure conditions. Two quartz windows were symmetrically mounted on opposite sides of the chamber to provide optical access, enabling the visualization and recording of spray development and flame evolution using a high-speed camera. In addition, the chamber body was equipped with a fuel injector, gas inlet and exhaust lines, a pressure sensor, and a temperature sensor to monitor and control the required experimental conditions inside the CVCC.

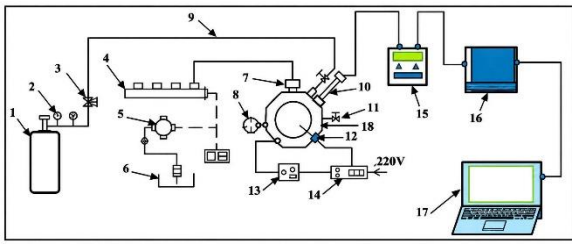


Fig. 1. Schematic diagram of the experimental setup

1. Nitrogen–oxygen mixture gas cylinder; 2. Compression pressure gauge; 3. Shut-off valve; 4. Common-rail accumulator; 5. High-pressure fuel pump; 6. Fuel tank; 7. Fuel injector; 8. CVCC pressure gauge; 9. Compressed air supply line; 10. AVL QC33C pressure sensor; 11. Exhaust gas line; 12. Thermocouple; 13. Voltage regulator; 14. Temperature controller; 15. AVL FLEXIFEM pressure measurement unit; 16. AVL IndiCom Mobile V2.9 software; 17. Computer; 18. Combustion chamber

To visualize the spray characteristics and combustion process, a high-speed optical imaging system was employed as shown in Fig. 2. During the spray experiments, a 300 W halogen lamp was used to provide sufficient illumination inside the CVCC, enabling clear visualization of the fuel spray against the background. For combustion experiments, the lamp was removed to avoid interference from external light with the measured flame luminosity. High-speed imaging was employed to capture the full evolution of the fuel spray and combustion processes.

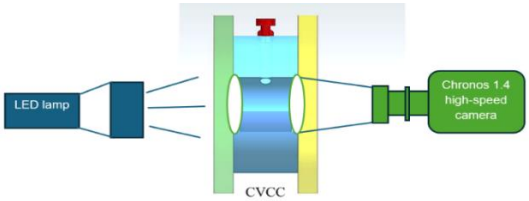


Fig. 2. Schematic diagram of the optical arrangement

2.2 Simulation of In-Cylinder Gas Conditions and Design Requirements of the Constant Volume Combustion Chamber

In diesel engines, the compression ratio (CR) depends on the method of air–fuel mixture formation to ensure reliable engine start under cold conditions. The minimum CR, ε = 13–16 is used for engines with open (undivided) combustion chamber, while ε = 17–21 is applied for engines with divided (pre-chamber) combustion chamber [6]. The end of compression pressure in naturally aspirated diesel engines ranges from 3 to 5 MPa with temperature of 750–950 K. The maximum cylinder pressure is approximately 6–9 MPa for naturally aspirated diesel engines, and up to 20 MPa for turbocharged diesel engines, while the maximum combustion gas temperature is typically in the range of 1700–2500 K [6-8]. The inner cylinder wall temperature must be kept below about 180 °C to prevent deterioration of the lubricating oil film. However, the peak temperature of 1700–2500 K represents the transient combustion gas temperature during the combustion process rather than the temperature of the combustion chamber wall. Owing to the very short combustion duration and heat transfer from the combustion gases to the chamber wall primarily through convection and conduction, the chamber wall temperature remains substantially lower than the combustion gas temperature. Therefore, in the present study, an inner wall temperature of 500 °C was adopted as the thermal loading condition for the finite element analysis. Similarly, a design pressure of 20 MPa was selected to represent the upper limit of the peak cylinder pressure in turbocharged diesel engines, thereby providing an adequate structural safety factor for the chamber design.

Table 1 summarizes representative CVCC systems that have been developed and employed in experimental studies. The chamber diameter ranges from 70 to 218 mm, with most optically accessible CVCC systems for spray and combustion investigations typically having chamber diameters of approximately 80–100 mm. A chamber diameter of 80 mm provides sufficient optical access for investigating spray tip penetration and spray cone angle, while maintaining a relatively compact chamber volume that improves heating efficiency, enhances temperature uniformity, and promotes air–fuel mixture formation [2]. Therefore, in the present study, a cylindrical combustion chamber with an inner diameter of 80 mm, a length of 90 mm, and a wall thickness of 60 mm was selected for the design and fabrication.

Table 1. Comparison of the geometrical characteristics, operating conditions, and combustion-condition generation methods of representative CVCC systems

Authors	Research focus	Heating / ignition method	Fuels	Chamber geometry			Surrounding conditions			Injection conditions	
				Ø (mm)	Depth (mm)	Volume (cm^3)	P_g (bar)	T_g (K)	ρ_g (kg/m^3)	P_i (MPa)	Nozzle Type
Baert *et al.* [9]	Spray and combustion	Pre-burn combustion	D	100	n.a	n.a	30	400-1,100	25.32	120	6 holes
Sandia National Laboratories (ECN) [10]	Spray, combustion, and soot	Pre-burn combustion	D, SME, OME, E	180	180	1,259	1-350	450-1,300	3-60	40-200	Single-hole/ multi-hole
Sieber *et al.* [11]	Combustion	Heated chamber gas	E, M	80	29	146	8-80	600-1,600	n.a	n.a	Pintle
Nguyen and Honnery [12]	Combustion	Spark ignition	D, BD, E	150	132	2,332	25	1,100	n.a	180	5 holes and single hole (0.2mm/hole)
Nguyen *et al.* [13]	Combustion	Spark ignition	H_2, NG	80	30	150	30-50	700-1,200	n.a	150	n.a.
Fujimoto *et al.* [14]	Soot behavior	Heated chamber gas	D	70	26	100	45	700-1,200	16.2	74.5	Single hole (0.2 mm)

Note: D=Diesel, E=Ethanol, M=Methanol, BD=Biodiesel, H_2=Hydrogen, NG=Natural, CNG= Compressed natural gas, SME=Soy methyl ester, OME=Oxymethylene Ethers, Ø: Chamber diameter, P_g: gas pressure, T_g: gas temperature, ρ_g: gas density; P_i: injection pressure

3. Constant Volume Combustion Chamber Design and Structural Strength Analysis

3.1. Design of the Combustion Chamber

Fig. 3 illustrates the main components of the developed CVCC system, including the chamber body, two quartz windows, chamber covers, and window flanges. As shown in Fig. 4, the chamber body was designed with an inner diameter of 80 mm, a length of 90 mm, and a wall thickness of 60 mm. These dimensions and the cylindrical configuration facilitate the installation of the experimental components while providing sufficient optical access for spray and combustion diagnostics. The chamber geometry also provides adequate space for integrating the fuel injector, electrical resistance heating system, compressed gas inlet and exhaust ports, and pressure and temperature sensors into a single experimental platform. The structural integrity of the combustion chamber under the design pressure and temperature conditions is evaluated in the following section.

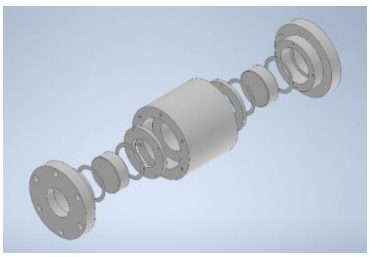


Fig. 3. Exploded view of the designed CVCC

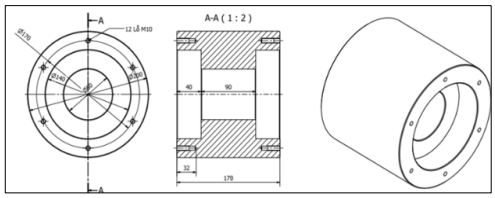


Fig. 4. Dimensions of the CVCC body

The chamber cover, illustrated in Fig. 5, is an intermediate component machined to connect the chamber body to the flanges. It is mounted between the chamber body and the flanges and provides structural support for the optical window assembly. The flanges were machined to accommodate the optical windows, with an outer diameter equal to that of the chamber cover and an inner diameter matching the outer diameter of the optical windows.

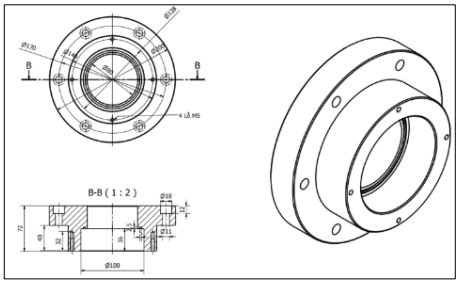


Fig. 5. Dimensional drawing of the CVCC cover

Carbon steel S45C was selected as the material for manufacturing the chamber body and flanges due to its high wear resistance, mechanical strength, and melting temperature [15]. For the optical windows, synthetic quartz was employed because of its superior mechanical strength and wide optical transmission range [16]. The flat quartz windows are cylindrical in shape, with an outer diameter of 100 mm and a thickness of 35 mm, as shown in Fig. 6. Table 2 and Table 3 list the material properties used in the design and simulation.

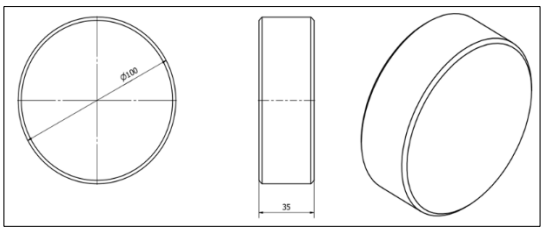


Fig. 6. Dimensions of the quartz window

Table 2. Material properties

Properties	Unit	Materials	
		Carbon steel S45C	Synthetic quartz
Density	kg /m^3	7,850	2,200
Young's modulus	GPa	205	-
Bulk modulus	GPa	-	31
Poisson's ratio	-	0.29	0.17
Tensile Strength, Ultimate	MPa	686	-
Tensile Strength, Yield	MPa	490	-
Elongation at Break	-	17%	-
Tensile strength	MPa	-	48
Compressive strength	MPa	-	1,103
Thermal Conductivity	W/(m.K)	49.8	1.4
Specific heat capacity	J/(kg.^{0}C)	486	670

3.2. Strength Analysis of the Constant Volume Combustion Chamber

3.2.1. Model setup and simulation conditions for the constant volume combustion chamber

In the finite element model, the full-scale combustion chamber assembly was initially evaluated to identify its baseline structural characteristics. Subsequently, to optimize

computational efficiency, a symmetric half model was adopted for detailed analysis, as illustrated in Fig. 7. In this model, the bolts were omitted and replaced by equivalent loads representing the bolt clamping force. The geometry was discretized using an automatic mesh generation algorithm with a mesh refinement strategy. To ensure solution accuracy, an element size of 3 mm was applied to the quartz windows, while a 5 mm size was used for the remaining components, including the chamber body and flanges. This approach effectively captures stress concentrations around the window interfaces while maintaining computational efficiency. The final model comprises 653,982 nodes and 346,592 elements.

Two simulation cases were considered to evaluate the thermal and structural performance of the proposed CVCC design. In the first case, a transient thermal analysis was conducted to determine the temperature distribution within the assembly. To achieve the target inner wall design limit of 500 °C, a thermal boundary condition was established by modeling an internal gas volume at 500 °C, while an internal gas pressure of 0.1 MPa was applied. A convection heat transfer coefficient of 50 W/(m^2·K) was adopted based on a previous study [17]. The resulting transient temperature field was used to assess the thermal response of the chamber components.

In the second case, a coupled thermomechanical structural analysis was performed under the design operating conditions. The temperature distribution obtained from the thermal analysis at 500 s was imported into the structural model as a thermal load. Simultaneously, an internal pressure of 20 MPa was applied to all internal surfaces of the chamber. Fixed supports were imposed at the window retaining interfaces, and equivalent bolt clamping forces were maintained. By combining the thermal and mechanical loads, the induced stresses and deformations were evaluated to verify the structural integrity of the proposed design. The Von Mises stress, principal stress, and total deformation were used as the primary assessment criteria.

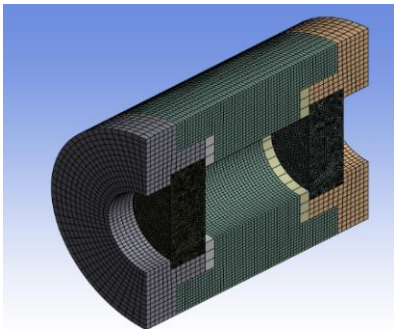
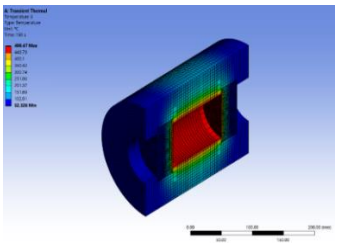


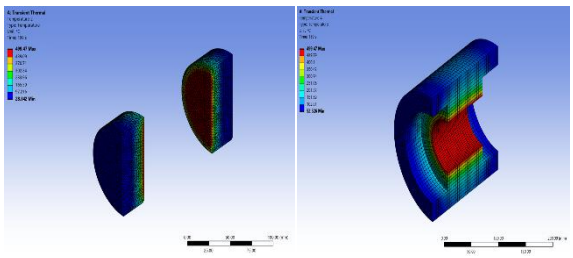
Fig. 7. Mesh generation results for the half CVCC model

3.2.3. Thermal analysis under high temperature conditions

The results indicate that the CVCC assembly reached a quasi-steady thermal state after 500 s, exhibiting a stable temperature distribution, as shown in Fig. 8a. To provide a more detailed examination, representative cross sections of the chamber body and the quartz window were analyzed, as shown in Fig. 8b and Fig. 8c, respectively. The results demonstrate a temperature gradient ranging from a maximum value of nearly 499.7°C at the internal surfaces, which is consistent with the applied thermal boundary condition of 500 °C, to a minimum value of 167.9 °C at the exterior walls. The quartz windows exhibit a maximum temperature of 499.8 °C at the inner contact surface and a minimum temperature of 116.0 °C at the outer edge. Additionally, the flange cover exhibits a temperature range from 340.6 °C at the interface with the combustion chamber to a minimum of 146.8 °C at the exterior mounting surface. Pronounced temperature gradients indicate efficient heat dissipation from the combustion region toward the external surfaces.

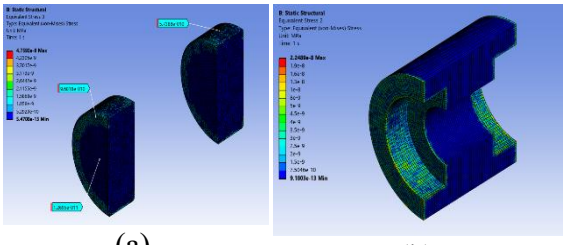


(a)



(b) (c)

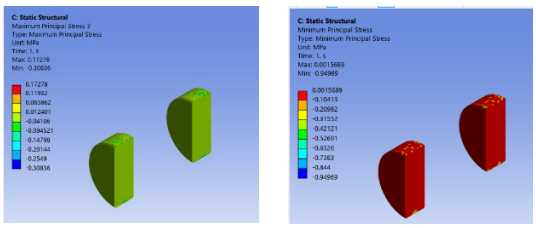
Fig. 8. Temperature distribution of the 1/2 CVCC model at 500 s: (a) overall assembly, (b) quartz window, and (c) chamber body



(a) (b)

Fig. 9. Von Mises stress distribution induced by thermal loading: (a) quartz window and (b) chamber body

The structural integrity of the CVCC assembly was evaluated under high-temperature operating conditions. The temperature distribution at 500 s, described above, was applied as a thermal body load, and an internal gas pressure of 0.1 MPa was applied as a mechanical load. Since the objective was to evaluate thermally induced stresses during the heating process, the internal pressure was assumed to represent ambient conditions prior to combustion. The analysis employed the Von Mises stress criterion for the metallic components and the principal stress criterion for the quartz windows to assess their susceptibility to brittle fracture. As illustrated in Fig. 9, the maximum Von Mises stresses were approximately 2.0 MPa and 4.7 MPa for the combustion chamber body and the flange cover, respectively. For the quartz windows, principal stress analysis indicated a maximum principal stress of 0.17 MPa and a minimum principal stress of −0.95 MPa. These values are well below the allowable stress limits of the material, confirming the structural safety of the windows, as shown in Fig. 10.



(a) (b)

Fig. 10. Principal stress distribution in the quartz window under thermal loading: (a) Maximum principal stress (σ_1) and (b) Minimum principal stress (σ_3)

Furthermore, the deformation induced by thermal loading was also evaluated. The results indicate that the assembly undergoes a maximum thermal deformation of 4.2×10^{-4} mm. As shown in Fig. 11, the highest displacement occurs at the interface regions between the metallic body and the quartz window, where the thermal gradients are most significant. In contrast, the exterior structural walls remain relatively stable, exhibiting negligible displacement. The extremely small deformation demonstrates the structural rigidity of the assembly and confirms that the design can effectively withstand thermal loads while maintaining the alignment and integrity of the internal components during high-temperature operation.

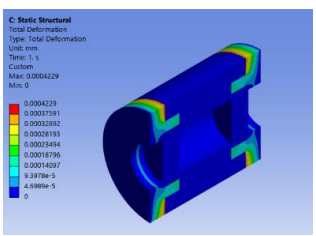


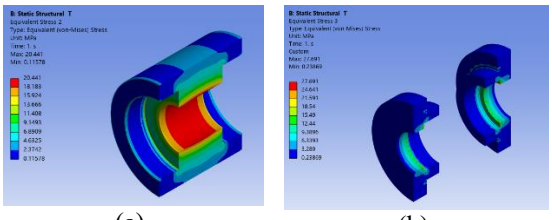
Fig. 11. Thermal deformation of the CVCC assembly

3.2.4. Structural Analysis under Combined Thermomechanical Loading

To evaluate the structural integrity under realistic operating conditions, a coupled thermomechanical analysis was performed by simultaneously applying an internal gas pressure of 20 MPa and the transient temperature distribution obtained at 500 s from the preceding thermal analysis. The structural responses of the chamber body, quartz windows, and flanges were evaluated to ensure that the induced stresses remained within the allowable limits of the respective materials. Frictionless support boundary conditions were applied to the assembly to represent the mounting constraints while allowing thermal expansion and promoting a realistic stress distribution.

As shown in Fig. 12a, the chamber body exhibits a maximum Von Mises stress of approximately 20.4 MPa. This value corresponds to only 4.2% of the yield strength of S45C carbon steel, as summarized in Table 2, indicating a substantial safety margin. Critical stress concentrations are observed at the internal walls subjected to direct pressure loading and near wall edges, where geometric discontinuities interrupt the load transfer path.

The structural response of the flange cover is presented in Fig. 12b. The maximum Von Mises stress is approximately 27.7 MPa, which remains significantly below the material yield strength of 490 MPa, as listed in Table 2. This corresponds to approximately 5.6% of the yield strength, confirming that the flange cover operates entirely within the elastic regime. Consequently, the component is expected to maintain adequate structural integrity and sealing performance under the specified thermomechanical loading conditions.



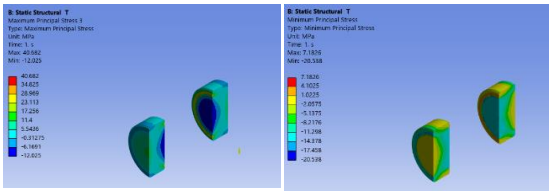
(a) (b)

Fig. 12. Von Mises stress distribution under combined thermomechanical loading: (a) chamber body and (b) flange cover

The structural integrity of the quartz window was evaluated by comparing the computed principal stresses with the characteristic strength properties listed in Table 2. As shown in Fig. 13a, the maximum principal stress (σ_1), which represents the tensile stress component, reaches a peak value of 40.7 MPa. This value remains below the tensile strength of quartz (48.0 MPa), indicating an adequate safety

margin against brittle fracture under the specified operating conditions.

Furthermore, as illustrated in Fig. 13b, the minimum principal stress (σ_3), representing the compressive stress component, reaches a maximum compressive value of −20.5 MPa. This stress level corresponds to only 1.8% of the compressive strength of quartz (1103 MPa), demonstrating an exceptionally large safety margin under compressive loading. Therefore, the quartz window is expected to maintain its structural integrity and resist brittle failure under the combined thermomechanical loading conditions.



(a) (b)

Fig. 13. Principal stress distribution in the quartz window under combined thermomechanical loading: (a) Maximum principal stress (σ_1) and (b) Minimum principal stress (σ_3)

These results confirm the structural robustness of the combustion chamber under combined thermomechanical loading. As shown in Fig. 14, the maximum total deformation of the assembly is 0.018 mm. The deformation distribution at the sealing interface is relatively uniform, with no significant localized deformation observed. The displacement difference between the bolt clamping locations and the adjacent contact regions is negligible. This uniform deformation profile prevents local separation of the mating surfaces, ensuring that the contact pressure remains above the level required to maintain an effective seal under an internal operating pressure of 20 MPa.

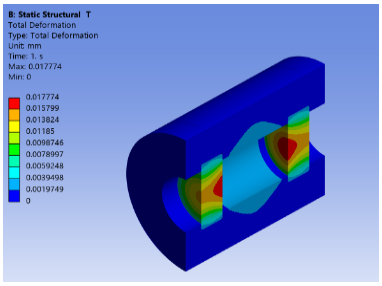


Fig. 14. Total deformation of the CVCC assembly under combined thermomechanical loading

4. Experimental Validation for Fuel Spray and Combustion Applications

4.1. Experimental Setup

Following the design calculations and structural integrity assessment using ANSYS, the CVCC system was fabricated and assembled as illustrated in Fig. 1. Diesel spray and combustion experiments were subsequently conducted to validate the performance of the developed system under conditions representative of compression ignition engines.

For the spray experiments, the initial chamber conditions were established at a temperature of 20 °C and a pressure of 4.0 MPa, while fuel was injected at injection pressures of 18 MPa and 20 MPa. For the combustion experiments, the initial chamber conditions were established at a temperature of 500 °C and a pressure of 4 MPa, with a fuel injection pressure of 20 MPa. Spray development and flame evolution were recorded through the quartz optical windows using a Chronos 1.4 high-speed camera. Meanwhile, the in-chamber pressure was continuously monitored using an AVL QC33C pressure sensor and acquired through an AVL FLEXIFEM data acquisition system for subsequent analysis. The experimental conditions used in the present study are summarized in Table 3.

Table 3. Experimental conditions

No.	Parameters	Test Conditions
1	Fuel	Diesel
2	Charge gas	20% Oxygen, 80% Nitrogen
3	Spray pressure (MPa)	18, 20
4	Initial chamber temperature (^{0}C)	20, 500
5	Initial chamber pressure (MPa)	4.0
6	Nozzle Diameter (mm)	0.19 (6-hole nozzle)
7	Recording speed (fps)	6000
8	Spray Time (ms)	2.5

4.2. Fuel Spray and Combustion Pressure Analyses

4.2.1. Diesel fuel spray analysis

For the spray experiments, the chamber was charged with a nitrogen–oxygen gas mixture (80% N_2 and 20% O_2 by volume) to an initial pressure of 4 MPa, while the chamber temperature was maintained at 20 ^{0}C. Fuel was injected using an electronically controlled common-rail injection system equipped with a Bosch six-hole injector with a nozzle diameter of 0.19 mm at injection pressures of 18 MPa and 20 MPa. Spray development was recorded through the quartz optical windows using a Chronos 1.4 high-speed camera. As observed in Fig. 15, a higher injection pressure resulted in an increased spray tip penetration (STP). This is because fuel

injected at a higher pressure possesses greater momentum, enabling the spray to penetrate further into the surrounding gas environment.

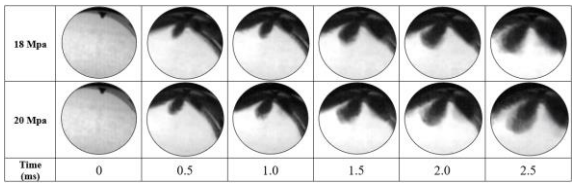


Fig. 15. Visualization of diesel fuel spray

4.2.2. Combustion characteristic

For the combustion experiments, the chamber was charged with a gas mixture to an initial pressure of 4 MPa and subsequently heated from 20 °C to 500 °C using a temperature control system. During the experiments, the in-chamber pressure was measured using an AVL QC33C pressure sensor, and the pressure data were acquired and analyzed using computer software. Flame development was recorded using a Chronos 1.4 high-speed camera operating at a frame rate of up to 38,500 fps.

Fig. 16 illustrates the diesel combustion process inside the constant-volume combustion chamber (CVCC). Shortly after fuel injection, auto-ignition occurred under the prescribed experimental conditions (500 °C and 4 MPa). The luminous flame region then expanded continuously from 0.5 to 2.5 ms. The rapid increase in flame area and luminosity indicates the high rate of chemical reactions and energy release immediately after the onset of auto-ignition. The occurrence of stable auto-ignition and continuous flame development demonstrates that the developed CVCC is capable of establishing thermodynamic conditions representative of compression-ignition engine operation. Furthermore, the clear visualization of flame evolution through the quartz optical windows confirms the stable operation of the developed system under elevated temperature and pressure conditions.

Fig. 17 shows the in-chamber pressure history and rate of heat release (ROHR) obtained during the diesel combustion experiment. The in-chamber pressure was measured using an AVL QC33C pressure sensor, while the ROHR was determined from the experimentally measured time-resolved in-chamber pressure history using the differential form of the first law of thermodynamics for a constant-volume combustion chamber. Before ignition, the chamber pressure remained nearly constant at approximately 4.0 MPa. Following ignition, the ROHR increased rapidly and reached its maximum value at approximately 4–5 ms, indicating the onset of intense combustion and rapid energy release. As a consequence of the heat released during combustion, the chamber pressure increased continuously from 4.0 MPa to approximately 4.73 MPa. After the peak heat release rate was reached, the ROHR gradually decreased due to fuel consumption, while the chamber pressure continued to rise at a lower rate as a result of the cumulative heat release. The pressure eventually approached a stable value after approximately 40 ms, indicating the completion of the main combustion phase. The pressure and heat-release histories are in good agreement with the flame development process shown in Fig. 16. These results confirm stable combustion and demonstrate that the developed CVCC can operate reliably under elevated temperature and pressure conditions, making it suitable for fuel spray and combustion studies under compression ignition engine relevant conditions.

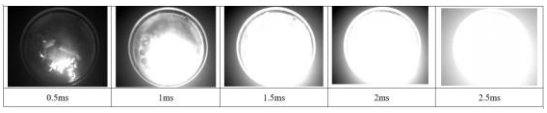


Fig. 16. Visualization of the diesel fuel combustion process at 500 °C

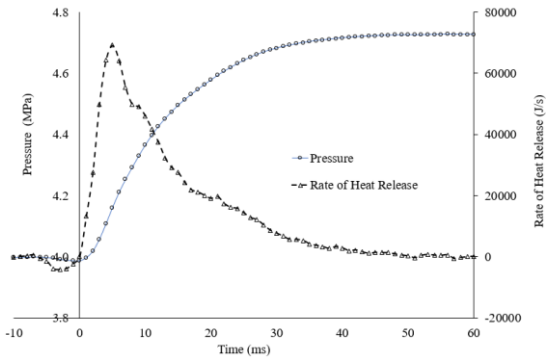


Fig. 17. In-chamber pressure history and rate of heat release

5. Conclusion

This study presented the design, development, and preliminary validation of a CVCC for investigating fuel spray and combustion processes under compression ignition engine conditions. Finite element analyses were conducted to evaluate the thermal and structural performance of the chamber under combined thermomechanical loading. The results showed that the maximum Von Mises stresses in the chamber body and flange cover were 20.4 MPa and 27.7 MPa, corresponding to only 4.2% and 5.6% of the yield strength of S45C steel, respectively. The maximum tensile stress in the quartz window was 40.7 MPa, remaining below its tensile strength of 48 MPa, while the maximum compressive stress was only 20.5 MPa, representing approximately 1.8% of its compressive strength. Furthermore, the maximum total deformation of the assembly was limited to

0.002 mm, ensuring adequate sealing performance under an internal operating pressure of 20 MPa.

Based on the design results, the CVCC was successfully fabricated and integrated with optical diagnostics, pressure measurement, heating, and common-rail fuel injection systems. Experimental investigations demonstrated stable fuel spray development and combustion under elevated pressure and temperature conditions. The measured pressure and heat release histories were consistent with the observed flame development process, confirming stable chamber operation and reliable data acquisition. These results demonstrate that the developed CVCC provides a controlled experimental platform for fundamental investigations of CI combustion and offers a flexible basis for studying fuel spray, ignition, combustion characteristics and the effects of alternative and low carbon fuels.

Acknowledgments

This work was supported by Hanoi University of Science and Technology (HUST) under the Grant T2024-PC-032.

References

[1] A. Hajialimohammadi, S. Ahmadisoleymani, A. Abdullah, O. Asgari, and F. Rezai, Design and manufacturing of a constant volume test combustion chamber for jet and flame visualization of CNG direct injection, Applied Mechanics and Materials, vols. 217–219, pp. 2539–2545, Nov. 2012. https://doi.org/10.4028/www.scientific.net/AMM.217-219.2539

[2] R. Munsin, C. Bodin, S. Lim, K. Phunpheeranurak, T. Phongphankasem, Y. Laoonual, S. Jugjai, and S. Chanchaona, Design of constant volume combustion chamber (CVCC) with pre-combustion technique for simulation of CI engine conditions, Proceedings of the 4th TSME International Conference on Mechanical Engineering (TSME-ICOME), Oct. 2013.

[3] M. Ul Haq, A. T. Jafry, S. Ahmad, and A. Muzaffar, Design and development of a control volume spray chamber (CVSC) for fuel spray visualization, Engineering Proceedings, vol. 23, no. 1, Art. no. 35, Aug. 2022. https://doi.org/10.3390/engproc2022023035

[4] V. T. Chau, T. D. Long, H. B. Vang, D. H. Long, and N. H. Huong, Design of a constant volume combustion chamber with optical approach technique, Journal of Science and Technology, vol. 64, no. 4, pp. 53–61, Sep. 2023. https://doi.org/10.46242/jstiuh.v64i04.4889

[5] N. P. Truong, N. X. Khoa, and N. V. Tuan, Building a research model for the combustion process of fuel in a constant volume combustion chamber, International Journal of Sustainable Engineering, vol. 17, iss. 1, pp. 263–277, Mar. 2024. https://doi.org/10.1080/19397038.2024.2329178

[6] N. T. Tien, Principles of Internal Combustion Engines, Hanoi, Vietnam: Education Publishing House, 2003. pp. 137-138

[7] J. B. Heywood, Internal Combustion Engine Fundamentals, New York, NY, USA: McGraw-Hill, p. 668, 1988.

[8] K. Mollenhauer and H. Tschöke, Handbook of Diesel Engines, Berlin, Germany: Springer, 2010, p. 539. https://doi.org/10.1007/978-3-540-89083-6

[9] R. S. G. Baert, P. J. M. Frijters, B. Somers, C. C. M. Luijten, and W. de Groot, Design and operation of a high pressure, high temperature cell for HD diesel spray diagnostics: Guidelines and results, SAE Technical Paper, no. 2009-01-0649, Apr. 2009. https://doi.org/10.4271/2009-01-0649

[10] Sandia National Laboratories, Combustion vessel geometry, Sandia National Laboratories, Diesel Spray Combustion Research, 2026. Online. Available: https://ecn.sandia.gov/diesel-spray-combustion/sandia-cv/combustion-vessel-geometry/, Accessed on: August 10, 2026

[11] D. L. Siebers and C. F. Edwards, Autoignition of methanol and ethanol sprays under diesel engine conditions, SAE Technical Paper, no. 870588, Feb. 1987. https://doi.org/10.4271/870588

[12] D. Honnery and D. Nguyen, Combustion of bio-oil ethanol blends at elevated pressure, Fuel, vol. 87, iss. 2, pp. 232–243, Feb. 2008. https://doi.org/10.1016/j.fuel.2007.04.023

[13] D. N. Nguyen, H. Ishida, and M. Shioji, Ignition delay and combustion characteristics of gaseous fuel jets, Journal of Engineering for Gas Turbines and Power, vol. 132, iss. 4, Apr. 2010. https://doi.org/10.1115/1.4000115

[14] H. Fujimoto, K. Higashi, T. Yamashita, and J. Senda, Effects of ambient temperature and oxygen concentration on soot behavior in diesel flame, SAE Technical Paper, no. 2005-24-007, Sep. 2005. https://doi.org/10.4271/2005-24-007

[15] MatWeb, JIS S45C Steel, Tempered, MatWeb, LLC, materials property database. Online. Available: https://www.matweb.com/search/datasheet_print.aspx?matguid=6b29957fc95e426d87dff64d67c59f6c, Accessed on: April 20, 2026

[16] Technical Glass Products, Quartz technical data, Technical Glass Products / 2SPI. Online. Available: Online. Available: https://www.2spi.com/catalog/documents/QuartzTechnicalData.pdf, Accessed on: April 20, 2026

[17] G. Chanakya and P. Kumar, Investigation of thermal adiabatic boundary condition on semitransparent wall in combined radiation and natural convection, International Journal for Computational Methods in Engineering Science and Mechanics, vol. 23, no. 4, pp. 349–366, 2022. https://doi.org/10.1080/15502287.2021.1964639